Coil Design for Neuromuscular Magnetic Stimulation Based on a Detailed 3-D Thigh Model

Stefan M. Goetz[1,2], Thomas Weyh[2], Ibrahim A. A. Afinowi[3], and Hans-Georg Herzog[2]

[1]Duke University, Durham, NC 27710 USA
[2]Technische Universität München, Munich 80333, Germany
[3]University of Sheffield, Sheffield S10 2TN, U.K.

Magnetic stimulation is gaining importance as an alternative to electrical stimulation in neurorehabilitation because it offers deep penetration and low pain. However, presently available equipment is not ideal for this purpose and sometimes even unsuitable. Furthermore, it is not known what physical conditions a coil has to provide for efficient stimulation. To solve these two problems, we set up a detailed 3-D computational model of the thigh to evaluate various coil designs with previously reported experimental performance. Comparison of the stimulation results with known experimental performance shows that a high absolute electric field seems to be sufficient for effective stimulation. Coil-generated field gradients, in contrast, do apparently not play a role. As a more appropriate metric, the electromagnetic coupling between different coil designs and the muscles of the thigh is found to be characteristic and explains the previously reported experimental performance differences. Furthermore, it is a good predictor for the achievable muscle torque (more than 99% correlation), whereas the gradient fails in this context. Accordingly, the model is able to test the performance of coils virtually and reveal both general relationships as well as design rules. In addition, the coupling factor formalism predicts a theoretical maximum level of the possible field induction and thus a guideline for potential improvements in the future.

Index Terms— **Activation mechanism, coil design, electromagnetic coupling, magnetic field design, magnetic stimulation, neuromuscular stimulation, rehabilitation engineering.**

I. Introduction

NEUROREHABILITATION for curing nerve lesions or treating after-effects has become a high-profile aim in neurology. The medical therapy of certain injuries, such as stroke, paraplegia, or other sources of paralysis, and multiple sclerosis, is often accompanied by physical therapy in combination with neuromuscular stimulation [1]. Such an approach reduces typical secondary effects of the lesion as it acts as a workout for the cardiovascular system and reduces atrophy. In addition, neuromuscular stimulation supports rehabilitation by its direct implications, especially relearning of movement sequences; reports suggest that this method can address neuromodulatory effects and brain plasticity [2]–[5]. Thus, from a medical perspective neuromuscular stimulation in rehabilitation may have very good prospects.

So far, electrical stimulation has been prevailing in that field [6]–[9]. However, this method—especially in the case of bigger muscles—can cause intolerable pain [10], [11]; such pain may significantly impede its success. Magnetic stimulation was suggested as an almost painless alternative. Due to the low attenuation of magnetic fields by the body, it furthermore allows a comparably deep penetration.

In early studies, muscle activation with magnetic stimulation is usually performed directly at a major nerve branch using a focal coil, such as the figure-of-eight design—the dominant shape in brain stimulation, where in contrast to here focality is usually wanted for selective stimulation—to evoke muscle contraction [12]–[15]. Such an approach entails two major disadvantages. First, this method requires a skilled person for finding the stimulation site and performing the procedure, whereas neuromuscular electrical stimulation is already a home-care tool for patients with the above-mentioned lesions. Second, the level of distress for strong responses is still unacceptably high. The underperformance of activating major nerves extramuscularly suggested to change the site of pulse application and to stimulate the intramuscular axon tree as homogeneously as possible instead [16]–[19]. In contrast to all expectations, the forces (e.g., for cycling) evoked by stimulation of the muscle venter with available equipment were relatively small, and the activation was not as uniform as desired.

In addition, the heating of the stimulation device and of the coil for the required repetitive pulse powers as well as for the long session durations turned out to be uncontrollably high. For a professional clinical application of neuromuscular magnetic stimulation, the equipment and the physical performance is accordingly the limiting factor. The techniques that allowed us to effectively handle the thermal issue in brain stimulation in the past are not sufficient here [20]–[24]. Instead, the essential goals are a more homogeneous activation and a higher energy efficiency.

A recent paper presented the potential of novel coil designs in a comparison of two magnetic stimulation coils with electrical stimulation for neuromuscular stimulation of the thigh in paretic rehabilitation patients [17]. One of the presented coils [Fig. 1(e)] was reported to improve the evoked muscle torque for the same stimulation amplitude by a factor of considerably more than 2.5 and even outper-

Manuscript received May 17, 2013; revised August 23, 2013; accepted January 9, 2014. Date of publication January 16, 2014; date of current version June 6, 2014. Corresponding author: S. M. Goetz (e-mail: sgoetz@tum.de).

Color versions of one or more of the figures in this paper are available online at http://ieeexplore.ieee.org.

Digital Object Identifier 10.1109/TMAG.2014.2300441

Fig. 1. Wiring profiles of the studied coils. (b)–(d) show commercial coils from MagVenture; (a) is the round coil with 15 turns (RND15) that was already compared with (e) in clinical studies [17], [19] and forms a good reference. Although this design is very similar to the MagVenture round coil (b) and does also not reflect the curved surface of the lower limbs, it has a slightly higher winding area. Coil (e) depicts an improved device which is already known from [17]. The curvatures on the longer side increase the field spread and produce a slight modulation. All coils are depicted with the same scale; the ruler with an overall length of 20 cm acts as a reference.

formed functional electrical stimulation. In these experiments, the electric fields in the muscle were lower than 80 V/m at the threshold; the administered maximum levels ranged up to almost 300 V/m at a biphasic pulse duration of 200 μs. These relatively short pulses compared with common magnetic stimulation devices, which usually generate pulses of more than 300 μs, are known to notably reduce the loss power [22]. The stimulation coil was placed directly on top of a muscle (Musculus quadriceps femoris). Whereas most other studies use traditional round coils or the so-called racetrack design, which owes its name to the winding shape [e.g., Fig. 1(d)], [17] tested the new geometry APL and compared it to the established mainstream equipment as well as to electrical stimulation. In addition, the up to then neglected question of coil positioning was studied there quantitatively. However, these experiments could not provide an explanation for the observed higher torque elicited by the improved coil. Another study extended the comparison to a number of different coil designs [25].

In this paper, we model and analyze the conditions of these experiments to understand and improve the performance of neuromuscular stimulation coils. The former aims at the physical field characteristic that may cause stimulation. Several excitation mechanisms have been proposed in [35]. These differ especially in the physical conditions they require for activation: a high-electric field amplitude versus a high gradient of the induced electric field. As a key task, the following accordingly has to fill the gap between the magnetic domain and the physiological effect, which is an essential requirement for both understanding and designing better equipment.

The model and the coil designs will be discussed in Sections II and III. A comparison with the quantitative experimental findings will entail important physical relationships for improving neuromuscular magnetic stimulation equipment. The first part of Section IV will show that the very distinct performance of the single coil designs is based on marked differences in their physical parameters. The electromagnetic coupling between the coil and the muscle tissue that surrounds the innervating axon tree, as derived in Section IV-C, seems to be suited best as a key figure that can describe the performance of a coil design. The unique feature of this theoretical formalism is that it allows even to predict the optimum that is achievable with any coil design.

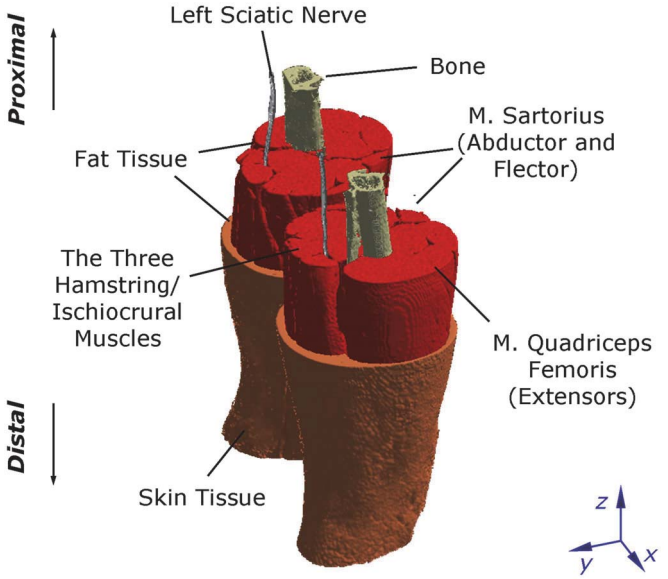

Fig. 2. High-resolution model of the thighs as used in the presented comparison with the knees located at the bottom end. The data were segmented and meshed based on a low-pass filtered (Gaussian filter with cutoff frequency of 1 mm^{-1} for the z-dimension and 4 mm^{-1} in the xy-plane) dataset to suppress imaging artifacts that could lead to unrealistically distorted boundary effects. In this depiction, the model was peeled to uncover the inner structure.

II. Methods

A. Model Description

A detailed 3-D model of the thigh was set up for the evaluation of various stimulation coils. The extensor muscles of the knee joint (i.e., Musculus rectus femoris, vastus lateralis, vastus intermedius, vastus medialis, manually defined in the model as the ventral part of the thigh from tendon to tendon) formed the region of interest (ROI). These are at present the key focus for clinical studies in neuromuscular magnetic stimulation for rehabilitation [12], [13], [16]–[18]. For this purpose, data from the Visible Human Project of the United States National Institutes of Health [26] were postprocessed and segmented. Comparable newer datasets are usually CT or MRI scans which provide either a limited tissue differentiation or poor spatial resolution. Therefore, we used the 70 mm photographs of cryosections that were prepared in the context of the Visible Human Project. The high resolution of the data allows the reconstruction of details, such as single blood vessels and extramuscular nerve branches among other tissue types, such as muscle, fat, skin, and bone. The resulting model consists of more than 20 million hexahedral volume cells in a regular grid (Fig. 2). The modeled body section with a length of 47.0 cm reaches approximately from the knee/patella to slightly below the hip/femoral neck. The dimensions of the thigh in x- and y-direction are approximately 16.5 cm and 18.8 cm, respectively.

The electrical characteristics for conductivity and permittivity are taken from the data of Gabriel *et al.* [27]–[29].

The specific electric properties of the single materials are assigned as follows: $\sigma = 0.34$ S/m, $\varepsilon_r = 5.2 \times 10^4$ for muscular tissue, 0.082 S/m and 8.4×10^2 for bone, 0.024 S/m and 2.8×10^3 for fat tissue, 2.0×10^{-4} S/m and 1.1×10^3 for the skin, as well as 0.31 S/m and 1.7×10^4 for blood vessels.

The model was solved under quasistationary conditions for a high-voltage oscillator frequency of 5000 Hz, which corresponds to a biphasic pulse duration of 200 µs as used in the experiments of [17] and [21]. The software is an established in-house package and applies the classical finite difference method to solve Maxwell's equations in potential formulation with linear eddy currents. The solution is performed in a two-stage process. The magnetic vector potential A at the location r is derived according to

$$\Delta A(r) = \mu j(r). \tag{1}$$

Because of the here spatially constant magnetic permeability μ, this equation is evaluated analytically using the Laplace operator's Green's function [30]. The induced electric field E is derived in a second stage by solving

$$\nabla \cdot (\kappa \nabla \phi(r)) = -i\omega A(r) \cdot \nabla \kappa \tag{2}$$

$$E(r) = -(i\omega A(r) + \nabla \phi(r)) \tag{3}$$

with the electrical potential ϕ, the complex conductance $\kappa := \sigma + i\varepsilon$, and $i^2 = -1$. Details of this typical approach can be drawn, for instance, from [31]. A current-insulating boundary condition was assigned to all surfaces.

The coils are incorporated as unmeshed wires [32], [33]. The current in the coils is predefined quasistationary and does not incorporate electromagnetic feedback from induced currents in the tissue. The latter is known to be vanishingly small in magnetic stimulation; the results and the coupling will reveal the correctness of this assumption. The simplification notably increases stability, which is an important issue in eddy-current simulation [34]. It also eliminates effects that are related to construction issues only, which are not of interest here, such as the proximity effect.

B. Metrics

The model is intended to answer two important questions. First, it should give insight into the mechanism that causes neuromuscular magnetic stimulation. The controversy regarding the activation mechanism of neuromuscular magnetic stimulation will be addressed by analyzing appropriate metrics for the electric field as well as its gradient (see Lines 3 to 5 in Table I) of various coils and comparing it to the experimental performance of these coils as reported in the literature.

Second, the coil comparison shall explain the performance differences also from an efficiency perspective and provide guidelines how the identified properties can be optimized to improve neuromuscular magnetic stimulation. For this purpose, further metrics for the intermediate stages between the coil current and the induced electric field, specifically the magnetic field energy and the induced electric energy in different segments of the model, are studied to track the energy conversion process step by step (Table I). These values shall characterize how well a specific coil targets the muscles and what portion of the energy generates merely unfavorable stray flux.

TABLE I
PHYSICAL QUANTITIES FOR EVALUATION OF COILS FOR NEUROMUSCULAR STIMULATION

Metric	Description
$\sqrt{\iiint_{V_{ROI}} \mathrm{B} \cdot \mathrm{H}\, d^3r}$	Magnetic Field Energy
$\sqrt{\iiint_{V_{ROI}} \int_{[0,T]} E \cdot j\, dt\, d^3r}$	Induced Electrical Energy
$\sqrt{\iiint_{V_{ROI}} \left\|\mathrm{E}_{xy}\right\|^2 d^3r}$	RMS Perpendicular Field
$\sqrt{\iiint_{V_{ROI}} \left\|\mathrm{E}_z\right\|^2 d^3r}$	RMS Longitudinal Field
$\sqrt{\iiint_{V_{ROI}} \left\|\frac{\partial \mathrm{E}_z}{\partial \mathrm{z}}\right\|^2 d^3r}$	RMS Longitudinal Gradient

C. Calculation of Coupling Factors

1) Motive: The electrical field distribution may show characteristic patterns of a specific coil, but especially with respect to two important questions it is either not sufficient or even not helpful at all and creates needs for another metric.

First, for rating and a quick comparison of coils, the induced electric field with its entire spatial distribution is not practical. The field profile or the induced energy, which can be derived from the former, may provide a well-defined guideline and could also be used as an objective for numerical optimization. However, both are secondary, phenomenological metrics which do not state obvious rules how an appropriate coil has to be designed; although the electrical field is influenced by the coil shape, its definition depends on many other physical quantities, such as the coil current, the frequency, or electrical properties of the target, which are not aspects of coil design.

Second, the electric field profile allows only a relative comparison between coils. For optimization and also from a scientific perspective, however, the physical limits are similarly important. A solution to this problem could lead to statements about the performance of a specific coil on an absolute scale and provide an estimate about limits for improvements in the future.

An appropriate theoretical concept from classical nonideal transformer theory, namely the coupling factor κ, can single out the geometric influence in the suboptimal induction process. The coupling factor splits efficiency into two parts: whereas the losses of the induction process of a transformer that are caused by the leakage flux are described by the coupling factor in a sufficient way, the other factors hindering a more efficient induction in magnetic stimulation, such as the high-electric resistance of biologic tissue, are eliminated. The latter, however, are not subject of coil design. Thus, the essential aspects can be analyzed separately.

2) Formalism: As generally known in electrodynamics and applied disciplines, e.g., power and communication engineering, the coupling factor links two inductances to one another from a macroscopical perspective. In the case of neuromuscular magnetic stimulation, these two inductances are given by

the stimulation coil and the ring currents in the muscle, which are coupled magnetically to each other.

The secondary current I_s in the muscle is described in dependence of the primary current I_p, i.e., the coil current, and three parameters, namely the inductance L_s of the secondary side and the tissue conductance X (containing capacitive and resistive contributions), as well as the mutual inductance M

$$M\frac{d}{dt}I_p = \left(X - L_s\frac{d}{dt}\right)I_s. \tag{4}$$

The back-action of the secondary side on the stimulation coil and its current I_p can be neglected as the secondary current is rather low and about six orders of magnitude smaller than the coil current in magnetic stimulation. Furthermore, the permeability of the tissue is nearly constant and approximately μ_0. The mutual inductance can therefore be expressed using the Biot–Savart solution of Ampère's law and be simplified as follows:

$$M \approx \frac{\Phi_c}{I_p} = \iint_{\Omega_s} \operatorname{curl}\left(\frac{\mu}{4\pi}\int_{\Gamma_p}\frac{d\boldsymbol{\gamma}_p}{\|\boldsymbol{\gamma}_\mathbf{p} - \mathbf{r_s}\|}\right)\cdot\frac{\partial \mathbf{r_s}}{\partial a}da \times \frac{\partial r_s}{\partial b}db \tag{5}$$

$$= \frac{\mu}{4\pi}\int_{\Gamma_s=\partial\Omega_s}\int_{\Gamma_p}\frac{d\boldsymbol{\gamma}_\mathbf{p}\cdot d\boldsymbol{\gamma}_\mathbf{s}}{\|\boldsymbol{\gamma}_\mathbf{p} - \boldsymbol{\gamma}_\mathbf{s}\|}. \tag{6}$$

Φ_c denotes the magnetic flux caused by the coil current I_p. Ω_s is the area encircled by the induced current which flows on the path Γ_s; this area is parametrized by $\mathbf{r_s}$. Γ_p is equivalent to the coil winding curve. The lower case symbols $\boldsymbol{\gamma}_\mathbf{p}$ and $\boldsymbol{\gamma}_\mathbf{s}$ denote position vectors on the paths determined by Γ_p and Γ_s, respectively. The coupling factor is most intuitively defined as the ratio of the inductances [30]

$$\kappa \equiv \frac{M}{\sqrt{L_p L_s}}. \tag{7}$$

Both κ and M are defined for closed loop paths along the induced current flow, thus 1-D manifolds, which are described by Γ_s here. For a distributed induced current density, a separate value for the coupling between the coil and the tissue can be assigned to each possible curve. The single paths can be derived from the vector field of the induced current density given by the numeric solution of the thigh model. Accordingly, the current density solution of the model is used for solving a second differential equation that in turn provides a set of integral curves representing Γ_s

$$\kappa = \lim_{h\to 0}\frac{\displaystyle\int_{\Gamma_\mathrm{S}}\int_{\Gamma_p}\frac{d\boldsymbol{\gamma}_\mathbf{1}ds}{\|\boldsymbol{\gamma}_\mathbf{1} - \boldsymbol{\gamma}(s)\|}\cdot\overbrace{\frac{\partial\gamma}{\partial s}}^{j(\gamma)}}{\sqrt{\displaystyle\iint_{\Gamma_\mathrm{P}^2}\frac{d\boldsymbol{\gamma}_\mathbf{1}\cdot d\boldsymbol{\gamma}_\mathbf{2}}{\|\boldsymbol{\gamma}_\mathbf{1} - \boldsymbol{\gamma}_\mathbf{2}\| + h}\iint_{\Gamma_\mathrm{S}^2}\frac{ds_1 ds_2}{\|\boldsymbol{\gamma}(s_1) - \boldsymbol{\gamma}(s_2)\| + h}\frac{\partial\boldsymbol{\gamma}}{\partial s}\Big|_{s_1}\cdot\frac{\partial\boldsymbol{\gamma}}{\partial s}\Big|_{s_2}}}. \tag{8}$$

The parametrization $\boldsymbol{\gamma}$ describes the integral curve along the induced tissue current density j through the starting point $p = \boldsymbol{\gamma}(s = 0)$ and replaces the fixed Γ_s from above. This Jordan path γ is chosen such that $j(\boldsymbol{\gamma}(s)) = (\partial\boldsymbol{\gamma}/\partial s|_{\boldsymbol{\gamma}})$. The parameter $0 \leq h \to 0$ is only required for a well-defined limit of the integrals. Alternatively, the integral paths can be guided around the singularities. The 120 000 starting points were evenly distributed throughout the muscle for each coil.

Practically interpreted, instead of using magnetic field energy ratios, (8) describes the coupling of a coil to the thigh or any other target in the body as the degree of matching between the coil conductor and the induced ring currents. This matching is primarily represented by the product of the two infinitesimal arc segments $d\boldsymbol{\gamma}_\mathbf{1}ds$ in the numerator, which describe the coil and the induced current locally, while it is inversely proportional to the distance between coil and target $\|\boldsymbol{\gamma}_\mathbf{1} - \boldsymbol{\gamma}(s)\|$. The denominator predominantly normalizes the inductances of the coil and the induced currents to compensate, for instance, the coil's number of turns and can be neglected for the interpretation.

III. Studied Coil Designs

Several coil designs were implemented in the model [Fig. 2]. For three of these devices [Fig. 2(a), (d), and (e)], accurate quantitative experimental data are available in [17], [19], and [25]. The design criterion for the muscle stimulation coil [Fig. 2(e)] was to achieve an optimum recruitment of the extensor muscles in the thigh and to avoid pain-inducing field peaks in the skin region, where the nociceptor density is high. The length, the width, and the curvature have been adapted to the observed spatial activation map as reported in [17]. The induced fields cover especially the most excitable parts of the quadriceps in the proximal half of the thigh. The inductance was tuned such that it matches the properties of clinically applied coils.

The coil designs were remodeled for this comparison based on geometrical data from X-ray images of the original devices. All coils were implemented with their exact characteristic winding patterns, i.e., in contrast to still common idealized geometric representations in magnetic stimulation models the single turns are accurately represented.

The relatively plain racetrack design [RT-120, Fig. 1(d)] from MagVenture (Copenhagen, Denmark) is momentarily the only available commercial coil specially designed for peripheral stimulation of whole muscles. For comparison only, the standard round [MC-125, Fig. 1(b)] and a figure-of-eight coil [MC-B70, Fig. 1(c)] of the same company were incorporated into this paper. Table II gives an overview over the coil designs; Fig. 1 displays their geometric characteristics. The model coils were placed on the thigh, based on the given optimum positions in [17]. In that experimental study, nine regions were defined on the surface and studied for their influence on (isometric) torque and distress. The strongest force responses were observed for stimulation in the first (proximal) third of the thigh with slightly lateral orientation. These optimum stimulation positions represent average optima among all subjects and may therefore still allow better individual locations. However, the positions were reported to be relatively consistent, and the variation of the torque with changing position was within the first half of the thigh relatively low (less than 9%) as long as the position was not medial. The high number of subjects with different training state and the wide covered age range from approximately

TABLE II
SPECIFICATIONS AND PROPERTIES OF SIMULATED COILS

Coil Measure	MagVenture MC-125 Fig. 1 (b)	MagVenture MC-B70 Fig. 1 (c)	MagVenture RT-120 Fig. 1 (d)	Rnd15 from [17] Fig. 1 (a)	APL from [17] Fig. 1 (e)
Winding Dimensions in mm	115	100 each	80 × 160	128	60 × 150 × 270
No. of Turns	13	2 × 10	10	15	8.5
Wire Length in m	3.1	4.1	3.4	3.5	5.2
Inductance in H	12	13	13	12	14

TABLE III
ANALYSIS RESULTS. VALUES ARE REPORTED FOR THE SAME PULSE ENERGY RELATIVE TO THE PERFORMANCE OF THE ROUND CIRCULAR COIL RND15, WHICH ACTED AS A REFERENCE IN SEVERAL PREVIOUS STUDIES [17], [19], [25]. PORTIONS ARE, ACCORDING TO THE ORDER OF MAGNITUDE, GIVEN IN PERCENT (%), PERMILL (‰), PARTS PER MILLION (PPM), OR PARTS PER BILLION (PPB). INDUCED ELECTRIC FIELD AND ITS ENERGY OF THE THREE TRADITIONAL ROUND COIL DESIGNS MC-125, RT-120, AND RND15 ARE RELATIVELY SIMILAR WHILE THE APL DESIGN CAN INDUCE ABOUT TWO-TIMES HIGHER FIELDS. ALTHOUGH THE MAGNETIC STRAY FLUX OF THE LATTER IS STILL ABOVE 85%, A PERCENTAGE OF MAGNETIC ENERGY PERVADING THE MUSCLES EXCEEDS THE TRADITIONAL COILS BY ABOUT A FACTOR OF TWO

Coil Measure	Magventure MC-125	Magventure MC-B70	MagVenture RT-120	RND15 from [17]	APL from [17]
RMS Perpendicular E-Field Muscle	0.82	0.29	0.70	1	1.29
RMS Perpendicular E-Field Adipose	0.83	0.38	0.68	1	1.35
RMS Longitudinal E-Field Muscle	0.82	0.60	0.81	1	2.14
RMS Longitudinal E-Field Adipose	0.84	0.63	0.82	1	2.14
RMS Longitudinal Gradient Muscle	0.88	0.91	0.71	1	1.39
RMS Longitudinal Gradient Adipose	0.90	0.92	0.71	1	1.39
Relative Induced Energy Muscle	0.68	0.17	0.54	1	2.62
Relative Induced Energy Adipose	0.69	0.24	0.55	1	2.88
Relative Induced Energy Femur	0.64	0.78	0.67	1	3.73
Percentage of Ind. Energy in Muscle	1.5 ppm	0.4 ppm	1.2 ppm	2.2 ppm	5.9 ppm
Percentage of Ind. Energy in Adipose	86 ppb	30 ppb	68 ppb	124 ppb	357 ppb
Percentage of Ind. Energy in Femur	6.9 ppb	0.8 ppb	7.0 ppb	10 ppb	39 ppb
Percentage of Mag. Energy in Muscle	5.7%	2.7%	3.9%	7.7%	14.8%
Percentage of Mag. Energy in Adipose	5.5%	4.1%	3.4%	7.0%	11.4%
Percentage of Mag. Energy in Femur	451 ppm	73 ppm	390 ppm	671 ppm	2583 ppm
Coupling Factor, Mean	1.47%	6.18‰	1.38%	1.59%	3.53%
Median	0.99%	3.04‰	1.00%	1.11%	2.64%
Quantile, 20%	0.56%	1.46‰	0.56%	0.63%	1.48%
Quantile, 80%	1.77%	6.00‰	1.75%	1.97%	4.68%
Log Mean	1.05%	3.22‰	1.02%	1.16%	2.68%

10 to 60 years, which contains the age of the visible human (38 years), recommends the positions as appropriate guidance for the model. In the simulations, the coils were accordingly placed (centrally) in the proximal half according to these earlier findings. The bigger APL device fully covers this range due to its wider outline. Fig. 4 illustrates coil placement.

IV. RESULTS AND ANALYSIS

A. Overview

The afore discussed physical metrics reported in Table I, which describe the induced electric and the magnetic field, are evaluated for the different segments of interest in Table III. For a fair comparison of coils with slightly different inductances, the metrics were not evaluated for equal current amplitude but for equal pulse energy. That step corresponds to a normalization to the same magnetic field energy and compensates also small differences of the corresponding inductances and gives free access to an unbiased analysis of the coil geometry.

From experiments, it is known that the APL design leads to about 2.6-times stronger responses than the round circular device RND15 [17], [25], whereas RND15 and the racetrack coil RT-120 evoke almost identical torque responses in the quadriceps femoris muscle [25]. Figure-of-eight coils are generally known to be absolutely unsuitable

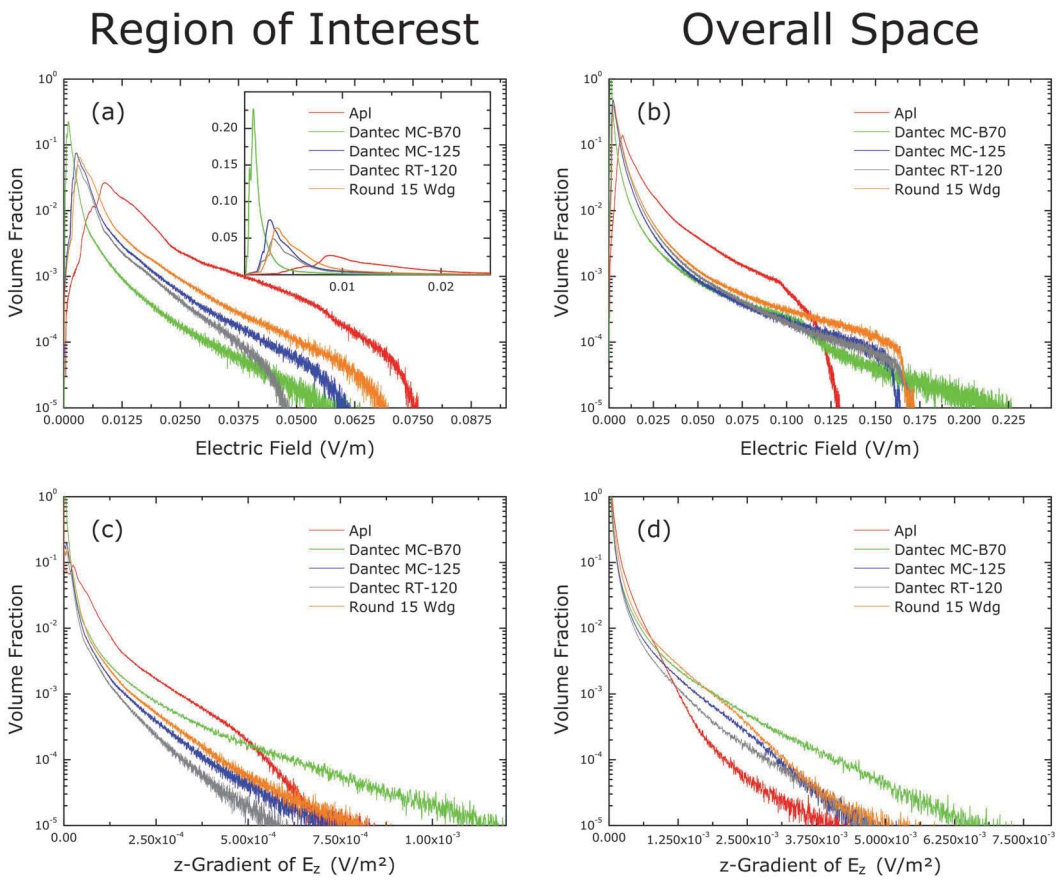

Fig. 3. Histograms of the induced electric field for a fixed current amplitude of 1 A. The graphs show the amplitude distribution in the ROI [quadriceps muscle group, (a) and (c) in left column] and the overall space [(b) and (d) in right column]. As anticipated, most space contains only a very low-electric energy. As the most focal device, the figure-of-eight coil presents the strongest electric field if the overall space is considered, but has the lowest field amplitude in the deep-lying ROI. This coil was added for elucidation of the principles and as a bench mark. For the second class of coils (round and racetrack coils) and especially for the APL design, the distribution peaks in the histogram for the ROI are shifted to notably higher amplitudes and show that these devices can pervade the target notably better. With respect to gradients, the figure-of-eight seems to outperform the round coils, revealing that the coil-generated gradient does not correlate with performance. The inset on top displays the data of the surrounding plot in a linear scale. The histograms are reported for a current amplitude of 1 A in all coils. Since the plotted quantities are directly proportional to the coil current so that the x-axes can be scaled to any other current amplitude.

for the stimulation of the intramuscular nerve tree and evoke only relatively low-muscle responses at high distress levels. A representative from this coil class was incorporated only as a reference since it can help to solve the question which mechanism of activation dominates neuromuscular magnetic stimulation.

In addition, from the computational perspective, the spatial distribution of the induced field in the ROI differs markedly between all studied coils [Fig. 4 and Table III]. The comparison of the values from Table III presents for the induced electric field and from an energy perspective (magnetically and electrically) three classes of coils. The round circular reference RND15, the slightly smaller MagVenture round circular coil MC-125 (dimensions in Table II), and the racetrack design RT-120 are very close to each other, reflecting also the experimental observations, and form the first class.

As a second class, the saddle-shaped APL coil, in contrast, induces notably higher electric fields (by a factor of 2.14 compared with RND15) and accordingly also an increased electrical energy (by a factor 2.62 compared with the reference).

The third class is represented by the figure-of-eight coil (MC-B70). It has the lowest values of induced electric field and induced electric field energy in the ROI. That is not surprising because this coil for brain stimulation was designed for maximum focality. The electric field is locally very strong but cannot permeate throughout a whole muscle; this high and focal peak of the induced electric field leads consequently to intense gradients of the latter. In contrast to the electric field, the gradient of the figure-of-eight coil—in longitudinal direction along the femur axis, the preferential orientation of the innervating nerves—averaged over the target muscle is competitive. It outperforms the round circular device MC-125 as well as the racetrack coil RT-120 and is just slightly smaller than that of the circular reference coil RND15; only the muscle stimulation coil APL leads to a stronger gradient.

The differences between the coil designs become clearer in the distribution plots. The histograms of the induced electric field strength are shown in Fig. 3. The right column shows the distributions of the amplitude over the whole space, the left column displays the corresponding metric for the ROI only.

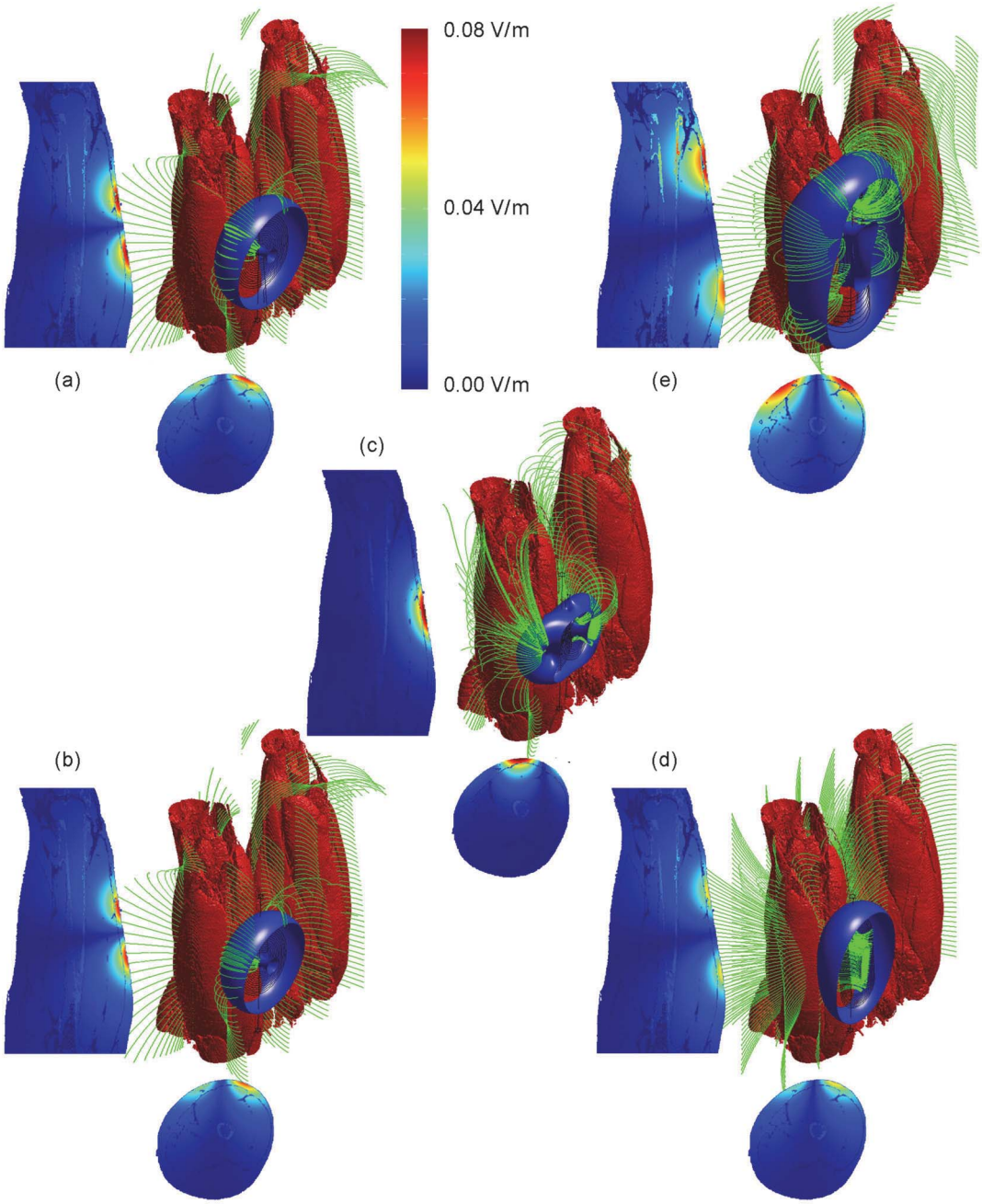

Fig. 4. Field plots of the studied coils. Every condition shows a cross section along the femoral axis (left) and a cross section with the peak electrical field in false color (in V/m for a coil current of 1 A as in Fig. 3). The 3-D plot depicts the muscular tissue (skin and fat stripped off) with the coil windings (dashed), field lines of the magnetic field (green), and an isosurface of the electric field (blue). Especially, the latter shows how confined the electrical field is around the figure-of-eight and also the round coils in contrast to APL. The denotation of the single coils is identical to the other figures [(a) RND15, (b) MC-125, (c) MC-B70, (d) RT-120, (e) APL].

As expected, all density functions are decreasing on average; i.e., high amplitudes are found only in a small part of the entire volume.

From the electric field histogram in the muscle in Fig. 3(a), the three classes from above are already separable by inspection: The curves of the round coils (RND15 as well as MC-125) and the racetrack design (RT-120) are shifted against each other but present similar shapes. The improved peripheral design APL [Fig. 1(e)] induces notably higher and more wide-ranging fields in the muscle. The figure-of-eight coil (MC-B70) induces only very low-field amplitudes in the muscle tissue. In the overall space [Fig. 3(b)], however, it generates the sharpest focus with highest amplitudes; this maximum is located in the immediate vicinity of the casing and does not extend into the muscle [see the field peak in the surface tissue layer in Fig. 4(c)]. Although much less pronounced, the class of round coils tends to similar extremes, whereas the improved APL design shows only marginal differences compared to the profile in the ROI [Fig. 3(a)].

The energy perspective reveals two facts (Table III): first, the comparison of the different coil types shows the same picture regarding performance as the field comparison. Second, the data indicate that the percentage of the total pulse energy that reaches the single body compartments in the form of induced currents is almost negligible. In addition to the influence of coil design, the poor energy transfer is caused by the high resistance of biologic tissues and will be addressed more rigorously in Section IV-C. Already on the stage of the magnetic field, only a small portion of the pulse energy reaches the target. According to Table III, the values range between 2% and 8%, only APL reaches almost 15%. None of these values is very competitive.

B. Activation Mechanisms and the Role of Gradients

In the peripheral nervous system, the gradients of the induced electric field are usually regarded as the contributions of the so-called activating function for stimulation [36], [37] leading to a stimulating current through the neural cell membrane due to current continuity. Such gradients can either be generated by the coil winding shape or they originate from the projection of a relatively homogeneous electric field on a nerve fiber. As discussed, the gradient strength of the induced electric fields shows a markedly different picture compared to the electric field strength induced by the single coils.

For the figure-of-eight coil in the ROI, the gradient values are only slightly smaller than those of the curve of the APL design and even higher than those of the second coil class (circular and racetrack coils), although it is commonly known that figure-of-eight coils are much weaker for the stimulation at the muscle venter and cause fundamentally more distress than round coils. As a consequence, the macroscopic, coil-generated gradient resulting from the geometry of the coil winding itself does not seem to cause stimulation to a sufficient extent. Otherwise, the performance of this coil type would have to be notably higher.

This may imply that from the two above-mentioned alternatives that have been proposed for nerve stimulation in general [35]–[38] the second seems to be dominant in the muscle: The macroscopic gradient caused by the coil winding shape, which might affect especially the comparably long axon branches of the first orders of the tree structure, seems to have a notably higher threshold and does not play a major role in the common device power range. On the basis of typical gradient values from the literature of more than 10^3 V/m^2 required for stimulation [35], even an optimistic estimation leads to a required coil current of more than 10 000 A for stimulation at the first branches of the intramuscular nerve tree because of the smoothing effect caused by the distance. However, it is known that already 1000–2000 A evoke a clear response of the thigh [17], [19].

Thus, neuromuscular stimulation does not activate the major nerve branches, which enter the muscles at the opposite side of the most common coil positions, but the important stimulation effect is expected to occur in the smaller branches of higher order. Due to the extremely fine spread of the intramuscular axon tree [39]–[43] with its bifurcations and turns, also homogeneous fields with sufficient amplitude are translated to impressive peaks of the projected gradient. This effect is known from the cortex where the electric field strength is claimed to be most important for activation [35], [44]. In combination with the dense tree of axons and motor terminals, which are dispersed over a relatively wide range [45]–[47], the key requirement for effective neuromuscular stimulation is accordingly a high-electric field.

C. Coupling

The pair-wise ratios between the coupling factors of the APL design, the standard round circular coil (RND15), and the racetrack coil (RT-120) reproduce the reported experimental performance characteristics from [17] and [21] relatively accurately. Compared with all other metrics from Table III, the coupling factor turns out to be the best predictor of the stimulation-evoked torque in the quadriceps muscle even if a linear homogenous regression model is applied. The correlation coefficient of the median reaches $\rho_c = 99.6\%$ and the weighted squared residual is $\chi_w^2 = 2.6 \times 10^{-3}$. The RMS-averaged electric field ($\rho_c = 98.9\%$, $\chi_w^2 = 8.2 \times 10^{-2}$) and the induced electric energy ($\rho_c = 98.5\%$, $\chi_w^2 = 3.0 \times 10^{-2}$) are both highly correlated as well, but slightly poorer predictors. For the gradient, however, the weighted residuals $\chi_w^2 = 0.15$—which are more than six times higher than those of the coupling factor—expose the seeming correlation ($\rho_c = 84.0\%$) as a merely spurious effect due to the high values of the APL coil, which dominate the fit. The regression with the gradient as the input parameter is not in good agreement with all the other coils. When the APL coil is left out, the correlation coefficient for the gradient would become even negative, whereas the coupling factor in this $(n-1)$ cross validation approach would be still correlated with more than 97%.

A higher coupling factor can be achieved in several ways. As long as no magnetic cores are incorporated into the system [48], [21], which can reduce the leakage flux, but also show some disadvantages in magnetic stimulation, the coupling factor is a geometric parameter. According to (8), it can be increased by enlarging the perimeter of the area that is spanned by the coil windings (numerator of the coupling integral on top). In addition, a lower distance $\|\boldsymbol{\gamma_1} - \boldsymbol{\gamma}(s)\|$, i.e., the distance between the coil and the induced ring currents in the target tissue, enhances κ with the inverse of the distance.

Finally, the coupling factor clarifies another important issue. Although the mean values of all coils are still very low, this cannot hide the fact that there exists a theoretical maximum at 1. This limit is hardly achievable on average in noninvasive magnetic stimulation due to the distance of the deeper parts of the muscles from the surface. However, none of the studied coils comes even close to it: none of them has a median coupling factor of more than a few percent, and also the 80% quantiles are not markedly higher. Also the APL coil, which was reported having the highest performance,

leaves with approximately 2.6% enough space for further improvements.

D. Basic Design Principles

From the findings discussed, the essential characteristics of a stimulation coil can be derived; these are also supported by the cited experimental observations. The key issue for neuromuscular stimulation is neither the gradient of the field nor focality, but a strong induced electric field that penetrates the muscle to the same extent as the nerves do. For this reason, the figure-of-eight design is inappropriate here. Likewise, relatively small circular coils and the studied racetrack design are too focal and do not provide a spatial distribution that is adapted to the target.

The most basic design rules recommend similarly spaced turns to avoid field peaks as well as maximizing the coupling factor between coil and target muscle tissue for a good induction process. As a rule of thumb, this implies that the shape should enclose a sufficient area which is bounded by the access surface of the target. As is well known from the rapid decay of the field with distance and also visible in the coupling formula, the gap between the winding and the target should be as small as possible. The increasing distance is a particular issue for high stacks of wires. Although the detrimental effects of high or multiple layers are in principle known [49], their effect may be underestimated. The commercial implementation RT-120, for instance, uses relatively high-conductor strips [Fig. 1]. The conductor height, however, shifts the current's barycenter away from the target. In an additional simulation, we reduced the height of the wires to the same value as used in RND15. For this hypothetical coil, the RMS longitudinal electric field in the muscle could be increased by approximately 10%, the induced energy by slightly more than 20%. The improved thermal behavior of the coil due to the increased conductor cross section may only in rare cases justify the performance degradation since there would be enough space in vertical direction. Although these basic guidelines sound trivial, there do still not exist persuasive designs in product catalogs of manufacturers or in the literature.

V. Conclusion

For the present paper, we set up a realistic anatomical model of the thigh, which represents one of the most studied peripheral neuromuscular stimulation targets. The physical analysis allowed us to explain previously reported performance differences of stimulation coils. Furthermore, the comparison with experimental data uncovered that the inherent field gradient of a coil itself seems to play a minor role; the conversion of absolute homogeneous fields into projected spatial derivatives and similar surface effects by the fine structures around the neuromuscular junction is much more efficient [50]. This aspect is highlighted by the figure-of-eight coil. Its gradient in the ROI was only slightly lower than that of the coil design with the highest performance and in the same league as the round as well as racetrack geometries. However, experiments show the inefficiency and high pain level of muscle stimulation with this design which is the dominant coil intranscranial applications. Thus, the field amplitude in the muscle tissue which surrounds the nerve tree might be the most important parameter.

The purpose-designed massive racetrack concept was inadequate. The simulation model revealed that for the thigh this geometry does not differ notably from a round design with respect to physical field characteristics [Fig. 3(a)]. This observation agrees well with previous experiments, which have shown that this coil type does not significantly differ from the round circular coil RND15 with respect to evoked forces in the quadriceps femoris muscle [25]. The cause for the underperformance is the extremely narrow shape. It leads to a spatial confinement of the magnetic (and induced electric) field and does not provide a substantial pervasion of the muscle. The gap in performance between the class of circular designs and the improved coil is accordingly still high.

Finally, we adopted the power-engineering concept of the coupling factor to eliminate irrelevant factors, such as specific electrical resistances or absolute inductance values, and reducing the complex field shape to a simple score. In addition to revealing an undistorted metric, it provides an absolute scale for coils' inductive performance and in this context also an absolute maximum. None of the analyzed coils exceeds a few percents. These figures motivate rigorous design reviews and novel approaches. Potentially clever flux guidance with magnetic materials at crucial places in contrast to massive steel-cores, which are too heavy for typical neuromuscular stimulation applications, may result in a further notable increase in coupling.

References

[1] T. Sinkjær and D. B. Popovic "Trends in the rehabilitation of hemiplegic subjects," *J. Autom. Control, Suppl.*, vol. 15, pp. 1–10, 2005.

[2] D. N. Rushton, "Functional electrical stimulation and rehabilitation—An hypothesis," *Med. Eng. Phys.*, vol. 25, no. 1, pp. 75–78, 2003.

[3] G. Lundborg, "Nerve injury and repair—A challenge to the plastic brain," *J. Peripheral Nervous Syst.*, vol. 8, no. 4, pp. 209–226, 2003.

[4] J. Netz, T. Lammers, and V. Hömberg, "Reorganization of motor output in the non-affected hemisphere after stroke," *Brain*, vol. 120, no. 9, pp. 1579–1586, 1997.

[5] L. G. Cohen, S. Bandinelli, T. W. Findley, and M. Hallett, "Motor reorganization after upper limb amputation in man. A study with focal magnetic stimulation," *Brain*, vol. 114, no. 1, pp. 615–627, 1991.

[6] S. Hamid and R. Hayek, "Role of electrical stimulation for rehabilitation and regeneration after spinal cord injury: An overview," *Eur. Spine J.*, vol. 17, no. 9, pp. 1256–1269, 2008.

[7] S. P. Hooker, S. F. Figoni, M. M. Rodgers, R. M. Glaser, T. Mathews, A. G. Suryprasad, *et al.*, "Physiologic effects of electrical stimulation leg cycle exercise training in spinal cord injured persons," *Archives Phys. Med. Rehabil.*, vol. 73, no. 5, pp. 470–476, 1992.

[8] J. S. Petrofsky and J. Smith, "Three-wheel cycle ergometer for use by men and women with paralysis," *Med. Biol. Eng. Comput.*, vol. 30, no. 3, pp. 364–369, 1992.

[9] L. R. Sheffler and J. Chae, "Neuromuscular electrical stimulation in neurorehabilitation," *Muscle Nerve*, vol. 25, no. 5, pp. 562–590, 2007.

[10] A. Delitto, M. J. Strube, A. D. Shulman, and S. D. Minor, "A study of discomfort with electrical stimulation," *Phys. Therapy*, vol. 72, no. 6, pp. 410–421, 1992.

[11] M. Schmelz, R. Schmidt, M. Ringkamp, H. O. Handwerker, and H. E. Torebjörk, "Sensitization of insensitive branches of C nociceptors in human skin," *J. Physiol.*, vol. 480, no. 2, pp. 389–394, 1994.

[12] K. Tomazin, S. Verges, N. Decorte, A. Oulerich, and G. Y. Millet, "Effects of coil characteristics for femoral nerve magnetic stimulation," *Muscle Nerve*, vol. 41, no. 3, pp. 406–409, 2010.

[13] V. Bustamante, A. Gorostiza, E. Lopez, and J. B. Gáldiz, "Magnetic stimulation of the quadriceps: Analysis of 2 stimulators used for diagnostic and therapeutic applications," *Archivos Bronconeumología*, vol. 43, no. 7, pp. 411–417, 2007.

[14] I. J. Kremenic, S. S. Ben-Avi, D. Leonhardt, and M. P. McHugh, "Transcutaneous magnetic stimulation of the quadriceps via the femoral nerve," *Muscle Nerve*, vol. 30, no. 3, pp. 379–381, 2004.

[15] M. I. Polkey, D. Kyroussis, C. H. Hamnegard, G. H. Mills, M. Green, and J. Moxham, "Quadriceps strength and fatigue assessed by magnetic stimulation of the femoral nerve in man," *Muscle Nerve*, vol. 19, no. 5, pp. 549-555, 1996.

[16] T.-R. Han, H.-I. Shin, and I.-S. Kim, "Magnetic stimulation of the quadriceps femoris muscle: Comparison of pain with electrical stimulation," *Amer. J. Phys. Med. Rehabil.*, vol. 85, no. 7, pp. 593–599, 2006.

[17] J. Szecsi, S. Götz, W. Pöllmann, and A. Straube, "Force-pain relationship in functional magnetic and electrical stimulation of subjects with paresis and preserved sensation," *Clin. Neurophysiol.*, vol. 121, no. 9, pp. 1589–1597, 2010.

[18] V. Bustamante, E. López, A. Gorostiza, U. Jiménez, and J. B. Gáldiz, "Muscle training with repetitive magnetic stimulation of the quadriceps in severe COPD patients," *Respirat. Med.*, vol. 104, no. 2, pp. 237–245, 2010.

[19] J. Szecsi, M. Schiller, A. Straube, and D. Gerling, "A comparison of functional electrical and magnetic stimulation for propelled cycling of paretic patients," *Archives Phys. Med. Rehabil.*, vol. 90, no. 4, pp. 564–570, 2009.

[20] T. Weyh, K. Wendicke, C. Mentschel, H. Zantow, and H. R. Siebner, "Marked differences in the thermal characteristics of figure-of-eight shaped coils for repetitive transcranial magnetic stimulation," *Clin. Neurophysiol.*, vol. 116, no. 6, pp. 1477–1486, 2005.

[21] H. W. Lorenzen and T. Weyh, "Practical application of the summation method for 3-D static magnetic field calculation of a setup of conductive and ferromagnetic material," *IEEE Trans. Magn.*, vol. 28, no. 2, pp. 1481–1484, Mar. 1992.

[22] S. M. Goetz, N. C. Truong, M. G. Gerhofer, A. V. Peterchev, T. Weyh, and H.-G. Herzog, "Analysis and optimization of pulse dynamics for magnetic stimulation," *PLoS One*, vol. 8, no. 3, p. E55771, 2012.

[23] S. M. Goetz, N. C. Truong, M. G. Gerhofer, A. V. Peterchev, H.-G. Herzog, and T. Weyh, "Optimization of magnetic neurostimulation waveforms for minimum power loss," in *Proc. IEEE 34th Annu. Int. Conf. EMBC*, vol. 34. Aug. 2012, pp. 4652–4655.

[24] S. M. Goetz, M. Pfaeffl, J. Huber, M. Singer, R. Marquardt, and T. Weyh, "Circuit topology and control principle for a first magnetic stimulator with fully controllable waveform," in *Proc. IEEE EMBC*, Aug./Sep. 2012, pp. 4700–4703.

[25] S. M. Goetz, H.-G. Herzog, N. Gattinger, and B. Gleich, "Comparison of coil designs for peripheral magnetic muscle stimulation," *J. Neural Eng.*, vol. 8, no. 5, p. 056007, 2011.

[26] M. J. Ackerman, "The visible human project," *Proc. IEEE*, vol. 86, no. 3, pp. 504–511, Mar. 1998.

[27] C. Gabriel, S. Gabriel, and E. Corthout, "The dielectric properties of biological tissues: I. Literature survey," *Phys. Med. Biol.*, vol. 41, no. 11, pp. 2231–2249, 1996.

[28] S. Gabriel, R. W. Lau, and C. Gabriel, "The dielectric properties of biological tissues: II. Measurements in the frequency range 10 Hz to 20 GHz," *Phys. Med. Biol.*, vol. 41, no. 11, pp. 2251–2269, 1996.

[29] S. Gabriel, R. W. Lau, and C. Gabriel, "The dielectric properties of biological tissues: III. Parametric models for the dielectric spectrum of tissues," *Phys. Med. Biol.*, vol. 41, no. 11, pp. 2271–2293, 1996.

[30] K. Küpfmüller, *Einführung in die Theoretische Elektrotechnik*. 3rd ed. Berlin, Germany: Springer-Verlag, 1965.

[31] M. Windhoff, A. Opitz, and A. Thielscher, "Electric field calculations in brain stimulation based on finite elements: An optimized processing pipeline for the generation and usage of accurate individual head models," *Human Brain Mapping*, vol. 34, no. 4, pp. 923–935, 2013.

[32] A. Abakar, G. Meunier, J.-L. Coulomb, and F.-X. Zgainski, "3D modeling of shielding structures made by conductors and thin plates," *IEEE Trans. Magn.*, vol. 36, no. 4, pp. 790–794, Jul. 2000.

[33] A. Abakar, J.-L. Coulomb, G. Meunier, F.-X. Zgainski, and C. Guérin, "3-D modeling of thin wire and thin plate using finite element method and electrical circuit equation," *IEEE Trans. Magn.*, vol. 37, no. 5, pp. 3238–3241, Sep. 2001.

[34] J. D. Lavers, "State of the art of numerical modeling for induction processes," *Int. J. Comput. Math. Electr. Electron. Eng.*, vol. 27, no. 2, pp. 335–349, 2008.

[35] J. Ruohonen, M. Panizza, J. Nilsson, P. Ravazzani, F. Grandori, and G. Tognola, "Transverse-field activation mechaniscm in magnetic stimulation of peripheral nerves," *Electroencephalogr. Clin. Neurophysiol.*, vol. 101, no. 2, pp. 167–174, 1996.

[36] F. Rattay, "Analysis of models for extracellular fiber stimulation," *IEEE Trans. Biomed. Eng.*, vol. 36, no. 7, pp. 676–682, Jul. 1989.

[37] P. J. Basser and B. J. Roth, "Stimulation of a myelinated nerve axon by electromagnetic induction," *Med. Biol. Eng. Comput.*, vol. 29, no. 3, pp. 261–268, 1991.

[38] F. Rattay, "Analysis of models for external stimulation of axons," *IEEE Trans. Biomed. Eng.*, vol. 33, no. 10, pp. 974–977, Oct. 1986.

[39] N. Guelekon, T. Peker, H. B. Turgut, A. Anil, and M. Karaköse, "Qualitative comparison of anatomical microdissection, Sihler's staining and computerized reconstruction methods for visualizing intramuscular nerve branches," *Surgical Radiologic Anatomy*, vol. 29, no. 5, pp. 373–378, 2007.

[40] T. Peker, N. Gülekon, B. H. Turgut, A. Anil, M. Karaköse, T. Mungan, *et al.*, "Observation of the relationship between the shape of skeletal muscles and their nerve distribution patterns: A transparent and microanatomic study," *Plastic Reconstruct. Surgery*, vol. 117, no. 1, pp. 165–176, 2005.

[41] V. A. Sheverdin, M. S. Hur, S. Y. Won, W. C. Song, K. S. Hu, K. S. Koh, *et al.*, "Extra- and intramuscular nerves distributions of the triceps surae muscle as a basis for muscle resection and botulinum toxin injections," *Surgical Radiol. Anatomy*, vol. 31, no. 8, pp. 615–521, 2009.

[42] T. Arakawa, S. Sekiya, K. Kumaki, and T. Terashima, "Intramuscular nerve distribution pattern of the oblique and transverse heads of the adductor hallucis muscles in the human foot," *Anatomical Sci. Int.*, vol. 81, no. 3, pp. 187–296, 2006.

[43] E. K. Dutton, C.-S. Uhm, S. J. Samuelsson, A. E. Schaffner, S. C. Fitzgerald, and M. P. Daniels, "Acetylcholine receptor aggregation at nerve-muscle contacts in mammalian cultures: Induction by ventral spinal cord neurons is specific to axons," *J. Neurosci.*, vol. 15, no. 11, pp. 7401–7416, 1995.

[44] Y. Tereao and Y. Ugawa, "Basic Mechanisms of TMS," *J. Clin. Neurophysiol.*, vol. 101, no. 2, pp. 167–174, 2002.

[45] X. C. An, J. H. Lee, S. Im, M. S. Lee, K. Hwang, H. W. Kim, *et al.*, "Anatomic localization of motor entry points and intramuscular nerve endings in the hamstring muscles," *Surgical Radiologic Anatomy*, vol. 32, no. 6, pp. 529–537, 2010.

[46] S. M. Aquilonius, H. Askmark, P. G. Gillberg, S. Nandedkar, Y. Olsson, and E. Stålberg, "Topographical localization of motor endplates in cryosections of whole human muscles," *Muscle Nerve*, vol. 7, no. 4, pp. 287–293, 1884.

[47] P. Wongphaet, K. Chinsethagij, S. Suarchawaratana, T. Dangpraesert, and W. Wongphaet, "Precise localization of motor branching and motor points: A cadeveric study," *J. Med. Assoc. Thailand*, vol. 88, no. 12, pp. 1884–1891, 2005.

[48] C. M. Epstein and K. R. Davey, "Iron-core coils for transcranial magnetic stimulation," *J. Clin. Neurophysiol.*, vol. 19, no. 3, pp. 376–381, 2002.

[49] F. S. Salinas, J. L. Lancaster, and P. T. Fox, "Detailed 3D models for the induced electric field of transcranial magnetic stimulation coils," *Phys. Med. Biol.*, vol. 52, no. 10, pp. 2879–2892, 2007.

[50] J. Ruohonen, *Transcranial Magnetic Stimulation: Modelling and New Techniques*. Espoo, Finland: Helsinki Univ. Technol., 1998.